

Deformation band formation and strength evolution in unlithified sand: The role of grain breakage

Bryan M. Kaproth,¹ Susan M. Cashman,² and Chris Marone¹

Received 18 January 2010; revised 2 July 2010; accepted 16 September 2010; published 16 December 2010.

[1] We report on laboratory experiments designed to investigate the strength evolution and formation mechanisms of cataclastic deformation bands hosted in unlithified sand, with particular focus on the role of grain breakage. Cataclastic deformation bands are characterized by particle size reduction and increased resistance to weathering compared to parent material. We recovered bands intact from late Quaternary, nearshore marine sand in the footwall of the active McKinleyville thrust fault, Humboldt County, California. Tabular samples 3–5 mm thick and 5 cm × 5 cm in area were sheared at normal stresses representative of in situ conditions, 0.5–1.8 MPa, sliding velocities from 10 $\mu\text{m/s}$ to 10 mm/s, and to shear strain up to 20. Cataclastic deformation bands are stronger than parent material (coefficient of internal friction $\mu_i = 0.623$ and $\mu_i = 0.525$, respectively) and exhibit a peak strength followed by weakening. Parent material exhibits significant strain hardening; the frictional yield strength increases up to 9% for a shear strain of 10. Detailed particle size analyses show that strain hardening in parent material is coincident with increased fine particle abundance, resulting from pervasive grain breakage. Our results support the hypothesis that cataclastic deformation bands are stronger than the surrounding parent material due to shear-driven grain breakage during their formation. We suggest that the combination of strain localization during band formation and strain hardening on individual bands results in dense networks of deformation bands.

Citation: Kaproth, B. M., S. M. Cashman, and C. Marone (2010), Deformation band formation and strength evolution in unlithified sand: The role of grain breakage, *J. Geophys. Res.*, 115, B12103, doi:10.1029/2010JB007406.

1. Introduction

[2] In response to shear strain, porous granular materials often fail in tabular zones referred to as deformation bands. We study deformation bands that exhibit shear offset and are characterized by grain size reduction and increased resistance to weathering relative to the unlithified sand in which they occur. These bands share characteristics of deformation bands described in sandstone [Fossen *et al.*, 2007], and thus, we refer to them as cataclastic deformation bands or alternatively cataclastic shear bands. Previous researchers have argued that strain hardening inhibits additional shear on such bands once they form, resulting in networks of closely spaced bands [Aydin, 1978; Mair *et al.*, 2000; Schultz and Balasko, 2003; Fossen *et al.*, 2007]. This hypothesis requires that cataclastic shear bands are stronger than their parent material and that the parent material strengthens in response to shear-driven cataclasis. While these components are generally consistent with existing data [e.g., Mair *et al.*, 2000], the hypothesis has not been adequately tested in laboratory experiments. The purpose of our study is to

present detailed laboratory measurements necessary to test this hypothesis and to combine measurements of frictional properties with particle size analysis to investigate the processes responsible for cataclastic shear band formation and strain hardening in poorly lithified sands.

[3] Cataclastic shear bands are best known in sandstone where estimated formation depths range from 1.5 to 2.5 km at 20–40 MPa effective lithostatic stress [Antonellini *et al.*, 1994; Fossen *et al.*, 2007]. These deformation bands localize along zones of parent rock that has been weakened [Mair *et al.*, 2000; Rawling and Goodwin, 2003], and deformation is often accommodated via cataclasis, with pervasive grain breakage. Cataclastic shear bands are commonly millimeters to centimeters thick and accommodate less than a few centimeters of shear displacement. Cataclastic deformation band formation has also been reported during laboratory studies conducted on sandstone at 34 MPa confining pressure [Mair *et al.*, 2000]. However, cataclastic deformation bands also occur at much shallower depths and confining pressures in unlithified materials [Cashman and Cashman, 2000; Wen and Aydin, 2004].

[4] Mair *et al.* [2000] presented a conceptual model for cataclastic deformation band formation in field and laboratory settings. They address the problem of localization in a strain hardening material; that is, how can strain localize in a zone that is adjacent to weaker material? In particular, they argue that the parent material must first weaken via cohesive

¹Department of Geosciences, Pennsylvania State University, University Park, Pennsylvania, USA.

²Department of Geology, Humboldt State University, Arcata, California, USA.

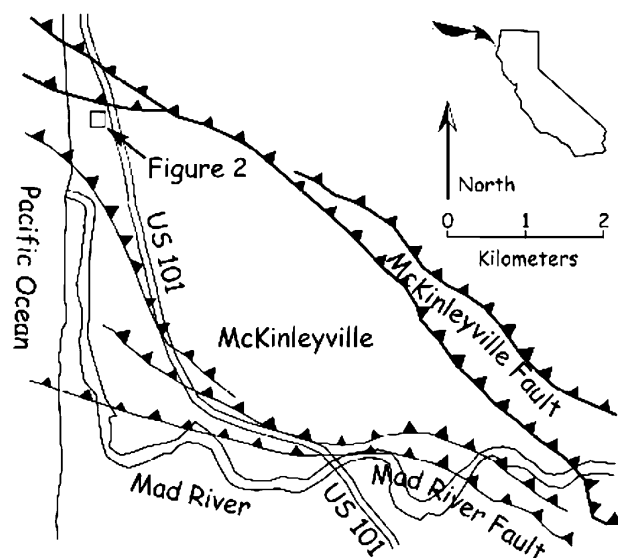


Figure 1. Map of site and fault surface traces near the McKinleyville area, California. Modified from *Cashman and Cashman* [2000].

breakdown in localized zones in order for deformation bands to form but that strain hardening processes terminate shear within such zones. In sandstones and in unlithified sands such as we studied, cataclasis seems to be an important process in both cataclastic shear band formation and shear termination, resulting in networks of closely spaced deformation bands. Previous workers have suggested that stress concentrations between bands promote the formation of step over cataclastic deformation bands, resulting in Riedel, ladder, and “radiator rock” arrays observed in the field [Schultz and Balasko, 2003].

[5] Recent theoretical work has been conducted to identify the formation conditions of different types of deformation bands [Wong et al., 1992; Zhu and Wong, 1997; Borja, 2004; Borja and Aydin, 2004; Wong et al., 2004; Aydin et al., 2006]. A cap plasticity model is preferred to describe these formation conditions [Fossen et al., 2007]. When the material crosses the yield surface or cap, a bifurcation occurs and a deformation band will begin to form. The type of deformation band that forms is dependent on the position in stress space at the time of failure [Wong et al., 1992; Zhu and Wong, 1997; Borja, 2004; Borja and Aydin, 2004; Wong et al., 2004; Aydin et al., 2006].

1.1. Field Site

[6] We collected cataclastic shear bands from an unlithified, late Pleistocene, nearshore-marine sand unit [Cashman and Cashman, 2000] in Humboldt County, California (Figure 1). This site is a ~150 m wide zone (Figure 2) that contains two varieties of deformation bands, dilation bands, and cataclastic shear bands [Cashman and Cashman, 2000; Du Bernard et al., 2002]. The parent material is well-sorted sand that contains abundant feldspar grains and lithic fragments. These deformation bands formed in response to slip on proximal strands of the seismically active McKinleyville thrust fault [Clarke and Carver, 1992; Cashman and Cashman, 2000].

[7] Maximum burial depth for the deformation bands we studied is less than 100 m, which corresponds to <1.8 MPa effective lithostatic stress. Burial depth is inferred from the stratigraphic context of the parent material unit: it is bounded by unconformities, a molar of the mastodon *Mammot americana* was found in the lowermost horizon of the unit (G.A. Carver, personal communication, 1993, cited by Harvey [1994]), a thermoluminescence age estimation of 176 ± 33 ka was determined for a mud horizon near the top of the unit [Berger, 1992], and the unconformably overlying 83 ka marine terrace [Carver and Burke, 1992] is currently ~33 m above sea level. Together, these features record the presence of the parent material unit at or above paleosea level multiple times in the late Pleistocene; there is no evidence of significant burial.

[8] Cataclastic shear bands occur in two conjugate sets (Figure 2), dipping at approximately 30° to the north and south, respectively [Cashman and Cashman, 2000; Du Bernard et al., 2002]. The majority of these bands are <1 cm thick and record reverse-fault shear displacement of a few millimeters to a few centimeters, corresponding to shear strains (γ) of <10 (Table 1). In a few cases, the bands are 10–20 cm thick and host a few meters of shear ($\gamma \approx 50$). Cataclastic shear bands at our study site weather in positive relief (Figure 2), indicating greater resistance and strength relative to their parent material. At our field site, dilation bands are generally 1–2 mm thick and subhorizontal and are spatially associated with cataclastic shear bands. Dilation bands are zones of increased granular porosity, which have become infilled with clay [Du Bernard et al., 2002].

[9] Relative to their parent material, our deformation bands are composed of finer and more angular grains and have decreased porosity (Figures 3 and 4; Table 1) [Cashman and Cashman, 2000]. Similarly, our experiments on parent material document cataclastic deformation with attendant compaction, as described below. These are identifiable characteristics of cataclastic shear bands formed in



Figure 2. Photograph of deformation bands expressed in relief at our field site. Deformation bands occur within unlithified, late Quaternary, nearshore marine sand in the McKinleyville Fault footwall (see Figure 1). Color streaks (subvertical) on the outcrop are due to the deposition of authigenic iron oxide minerals in pore space. Outcrop faces west; north is to the left in this photograph. Note pencil for scale.

Table 1. Physical Properties of Cataclastic Shear Bands and Parent Material Collected From the Study Site

Sample	Offset (mm)	Thickness (mm)	Shear Strain	Porosity (%)	Mean Grain Size (μm)	Skewness
Parent material	na	na	na	44–47	200	0.29
08C05	80	12.5	6	25	35	0.98
C06	unkn	100	unkn	27.5	103	0.90
08B04	70	9.0	8	30.5	45	0.95
08B03	2500	50	50	24.5	50	0.94

sandstone; hence, we use that term here. Unlike *Aydin et al.* [2006], we argue that these bands have undergone significant grain breakage to accommodate shear. Grain breakage results in a wide particle size distribution (PSD) relative to the parent material (Figure 3) and is consistent with the observations of *Rawling and Goodwin* [2003].

1.2. Strength of Cataclastic Shear Bands

[10] We measured the frictional shear strength of cataclastic shear bands and their parent material. In addition, we analyzed the evolution of parent material strength and PSD as a function of shear strain. We specifically assessed the effect of grain breakage on parent material strength. Shear-driven grain breakage may enhance material strength as a result of increased grain angularity [e.g., *Zhu et al.*, 1997; *Cresswell and Barton*, 2002; *Mair et al.*, 2002; *Anthony and Marone*, 2005; *Guo and Morgan*, 2006], pore collapse [*Knudsen*, 1959; *Aydin*, 1978], and changes in PSD [*Lambe and Whitman*, 1969]. Cementation may also play an important role in deformation band evolution.

1.3. Permeability and Fluid Flow

[11] Deformation bands have received significant attention due to their influence on fluid flow and reservoir systems [*Zhu and Wong*, 1997; *Aydin*, 2000; *Lothe et al.*, 2002; *Parnell et al.*, 2004; *Perez et al.*, 2010]. The porosity of cataclastic shear bands relative to parent material can be reduced by an order of magnitude or more. The permeability of these bands may be anisotropic and significantly lower than parent material [*Antonellini et al.*, 1994; *Zhu and Wong*, 1997; *Lothe et al.*, 2002; *Fossen et al.*, 2007]. Within a cataclastic shear band, permeability reduction is a result of PSD changes, tighter packing, intergrain crack closure, increased tortuosity, and, in some cases, pore collapse immediately outside the band. Laboratory measurements of permeability perpendicular to our cataclastic shear bands are 1–3 orders of magnitude lower than that of parent material [*Perez et al.*, 2010]. At our field site, the preferred orientation of colored streaks, authigenic iron oxide deposits, is altered near the deformation bands (Figure 2), indicative of their effect on fluid flow.

2. Methods

[12] We identified cataclastic shear bands for collection along an actively eroding sea cliff that exposes the unlithified, late Pleistocene parent material unit (Figure 1). To expose unweathered bands for collection, the outcrop surface was removed using hand tools. Individual bands were extracted and sealed in plastic wrap to preserve sample moisture and integrity. Our suite of samples represents cataclastic deformation bands over a range of shear displacements, orientations, and thicknesses (Table 1).

2.1. Sample Characterization

[13] At the field site, we measured thickness and apparent displacement of the cataclastic shear bands. Shear displacement was constrained by apparent lateral offset of sedimentary strata and other bands. Shear strain was estimated by dividing the apparent offset by the band thickness (Table 1).

[14] Figure 3 shows particle size distributions for bands and parent material. To highlight differences between samples, we calculated inclusive graphic skewness λ [after *Folk and Ward*, 1957], using the mean size of the parent material (205 μm) in lieu of the mean size of the material of interest. In this scheme, a PSD skewed toward fine particles has a greater skewness.

[15] Porosity (ϕ) of intact bands and parent material was calculated from bulk density and solid density, following $\phi = 1 - (\rho_b/\rho_s)$ (Table 1). The solid density ρ_s was measured by weighing a sample and then measuring its displacement in water, allowing the water to permeate the pore space. The bulk density ρ_b was measured by weighing a sample, applying a waterproof acrylic coating, then measuring its displacement in water, preventing the water from permeating the pore space. We assume that the density difference between ρ_s and ρ_b is due to pore space.

2.2. Laboratory Sample Preparation

[16] Layers 3–5 mm thick and 5 cm \times 5 cm in area were extracted from the field samples for laboratory experiments.

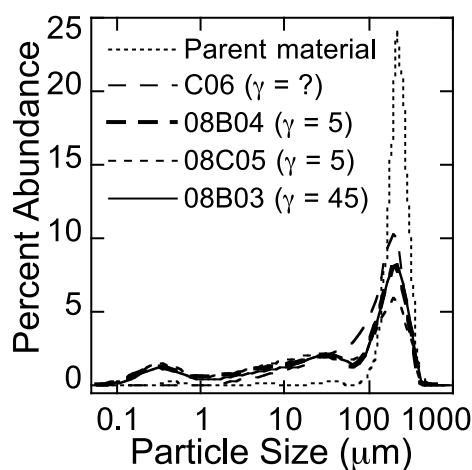


Figure 3. PSDs of parent material and cataclastic shear bands. Shear strain is indicated as γ (unknown for sample C06). PSDs were determined using a Malvern Mastersizer S (dynamic particle size range from 0.05 to 900 μm). See Table 1 for other details of sample characteristics.

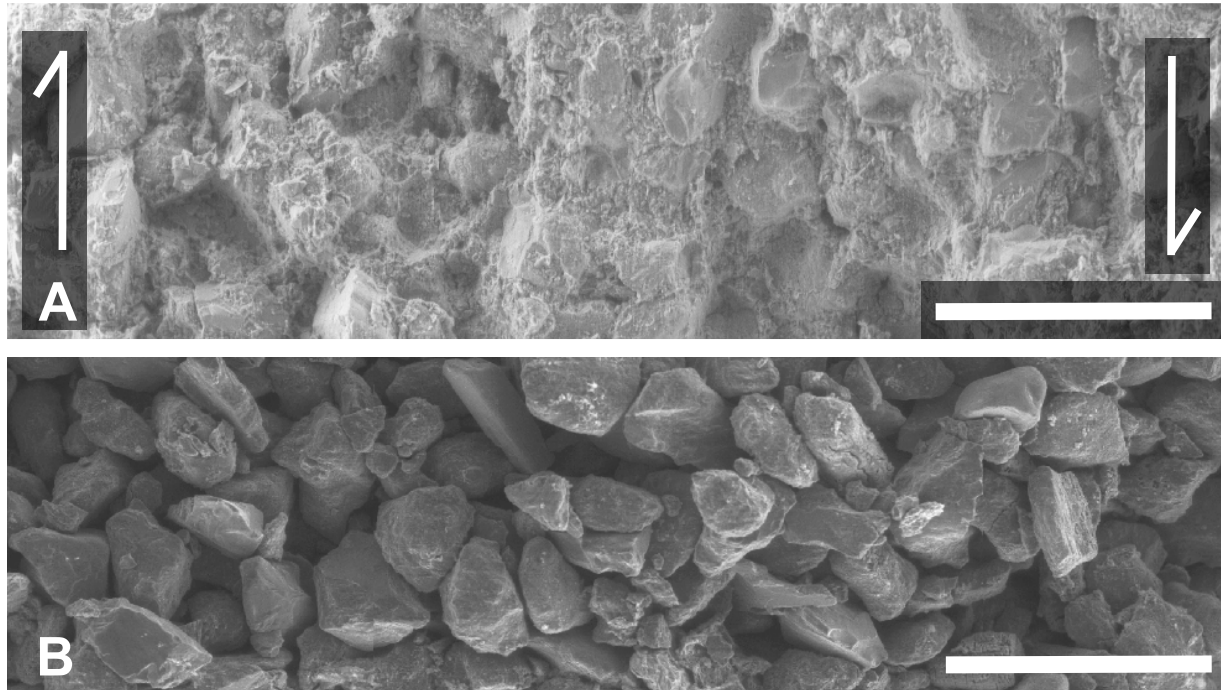


Figure 4. SEM images of (a) cataclastic shear band 08B03 ($\gamma = 50$) and (b) parent material as recovered in the field. The arrows denote sense of shear. Scale bars, 500 μm .

For most bands, we were able to recover multiple layers, which were used to assess experiment reproducibility and in parametric studies of strength as a function of experimental variables such as normal stress (Table 2). Layers were first rough cut and then trimmed to specific layer dimensions with a hand-held, precision rotary sander. Layers of loose parent material were constructed to specific layer dimensions in a leveling jig. Layers were oven dried prior to shear (100°C , >30 min) for dry experiments or presaturated with tap water for saturated experiments.

2.3. Laboratory Techniques

[17] We conducted friction experiments in a servo-controlled biaxial testing apparatus (for details, see *Anthony and Marone* [2005], *Savage and Marone* [2007], or *Rathbun et al.* [2008]). Sample layers were sheared in a three-forcing block configuration using either double-direct shear (DDS) or single-direct shear (SDS; Figure 5). For DDS experiments, two layers were sheared simultaneously. For SDS experiments, a low friction bearing was used in place of one layer [e.g., *Marone*, 1995; *Marone et al.*, 2008]. Normal stress on the layers was maintained constant via a fast acting servo-hydraulic controller. Layers were sheared by driving the central block of the sample assembly down at a controlled rate, typically 10 $\mu\text{m/s}$. Shear and normal stresses were measured with strain gauge load cells accurate to ± 0.1 kPa, and displacements were measured with direct current displacement transducers (DCDTs) accurate to ± 0.1 μm . All stresses and displacements were recorded digitally at 10 kHz with a 24-bit system and averaged to 10–100 Hz for storage.

[18] We compared the strength of cataclastic deformation bands and parent material using the SDS configuration (Figure 5a and Table 2). This configuration required minimal sample material and was used to maximize data from a limited number of samples.

[19] Experiments conducted with the DDS configuration were designed to assess the effect of grain breakage and changes in PSD on parent material strength. This suite of experiments was conducted on parent material at constant normal stress ($\sigma_n = 0.75$ – 1.75 MPa), moisture conditions (dry, saturated), and driving velocity (10–10,000 $\mu\text{m/s}$) to variable final shear strains ($\gamma = 0.5$ – 20 ; Table 3). We measured PSD at the beginning and end of all experiments. Initial layer thickness was measured with calipers to ± 50 μm . Change in layer thickness was measured during each experiment and was corrected for geometric thinning [e.g., *Scott et al.*, 1994]. We used layer thickness change to assess PSD changes during an experiment, assuming that poorly sorted PSDs can compact more than well-sorted distributions. Details of the layer thickness change as a function of shear indicate a combination of shear driven dilation and compaction [e.g., *Mair et al.*, 2002; *Anthony and Marone*, 2005; *Rathbun et al.*, 2008].

[20] All experiments began with a shear displacement of 5 mm at a normal stress of 0.5 MPa. This “run-in” was designed to minimize differences in initial packing state and to develop a consistent initial fabric [e.g., *Marone*, 1998]. Our data include measurements of the bulk shear strain, derived by integrating the incremental shear displacement divided by the instantaneous layer thickness. At the end of all experiments, shear stress and normal stress were removed, and the deformed layers were collected. Residual sample

Table 2. Single-Direct Shear Experimental Parameters^a

Experiment	Material	σ_n (MPa)	τ_f (MPa)	μ_f
p1791	parent material	0.5	0.293	0.602
p1752	parent material	0.5	0.309	0.614
p1982	parent material	0.75	0.450	0.604
p1976	parent material	0.75	0.463	0.622
p1981	parent material	0.75	0.475	0.634
p1792	parent material	1	0.581	0.571
p1785	parent material	1	0.611	0.576
p1752	parent material	1	0.593	0.584
p1791	parent material	1	0.563	0.568
p1788	parent material	1	0.577	0.576
p2163	parent material	1.25	0.673	0.540
p1980	parent material	1.25	0.717	0.566
p2299	parent material	1.4	0.732	0.522
p2298	parent material	1.5	0.811	0.525
p2297	parent material	1.5	0.784	0.509
p1794	parent material	1.8	0.998	0.558
p1793	parent material	1.8	1.026	0.572
p1871	parent material	1.8	1.070	0.596
p1795	parent material	1.8	0.989	0.551
p1789	C06	0.5	0.354	0.698
p1751	C06	0.5	0.331	0.655
p2161	08B03	0.75	0.489	0.651
p1979	C06	0.75	0.489	0.647
p1977	C06	0.75	0.478	0.662
p1978	C06	0.75	0.487	0.647
p1979	C06	0.75	0.490	0.646
p1978	C06	0.75	0.487	0.662
p1920	C06	0.75	0.478	0.637
p1786	C06	1	0.671	0.663
p1789	C06	1	0.627	0.634
p1751	C06	1	0.676	0.677
p2159	C06	1.25	0.800	0.643
p2157	C06	1.5	0.873	0.584
p2155	C06	1.5	0.880	0.588
p1919	08B03	1.8	1.068	0.592
p1877	08B03	1.8	1.138	0.632
p2022	08B04	1.8	1.105	0.616
p2024	08C05	1.8	1.141	0.635
p2026	08C05	1.8	1.154	0.643
p2025	C06	1.8	1.132	0.630
p1876	C06	1.8	1.153	0.638
p1790	C06	1.8	1.242	0.691
p2021	08B03	1.85	1.125	0.609

^aExperiments were conducted on dry parent material and cataclastic shear bands at constant sliding velocity (10 $\mu\text{m/s}$) and normal stress (0.5–1.85 MPa). We report the maximum shear stress (τ_f) and friction (μ_f) at the initiation of permanent shear deformation.

wafers from the saturated experiments were sectioned for SEM analysis. Sample collection was not possible for dry experiment because the layers lacked cohesion.

3. Experiment Results

[21] Cataclastic shear bands have distinctly different frictional histories than parent material (Figure 6). Upon shear loading, all materials exhibit an initial increase in stress associated with elastic loading of the layer, followed by permanent inelastic shear deformation, consistent with previous observations [e.g., *Feda, 1982; Bonn and Denn, 2009*]. Cataclastic shear bands typically yield at higher shear stress than parent material. Following yield, parent material often exhibits strain hardening. In contrast, cataclastic shear bands exhibit a peak stress followed by weakening. In general, steady state strength of the bands

was 90%–97% of the peak stress and was attained after a shear strain of ~ 1 –2.

3.1. Comparison of Cataclastic Shear Bands and Parent Material

[22] Cataclastic shear bands are stronger than parent material under all of the conditions we studied (Figure 7). Coulomb-Mohr failure envelopes were determined by fitting our measurements with the relation $\tau_f = \mu_i \sigma_n + c_0$, where μ_i is the coefficient of internal friction, σ_n is normal stress on our layers, c_0 is cohesion, and τ_f is the maximum shear stress at the initiation of permanent shear deformation. Herein τ_f is defined as the maximum shear stress over the interval from the yield point to an additional shear strain of 1. Figure 7 shows that cataclastic shear bands ($\mu_i = 0.623$, $c_0 = 22$ kPa) have greater internal friction and similar cohesion compared to parent material ($\mu_i = 0.525$, $c_0 = 48$ kPa); see also Table 2. Field evidence indicates that cataclastic shear bands have greater cohesive strength than parent material, given their increased resistance to weathering (Figure 2); however, the magnitude of this difference is apparently within our experimental measurement uncertainty.

[23] The strength of parent material generally increases as a function of shear strain (Figure 6), and such strain hardening is observed under all experimental conditions (e.g., normal stress, sliding velocity, dry/saturated). The degree of strain hardening is variable, with sliding friction increasing by 0–1% per unit increase in shear strain, but it is consistently positive when averaged over shear strain greater than ~ 0.2 . Over a full experiment the strength of parent material approaches but seldom reaches cataclastic shear band

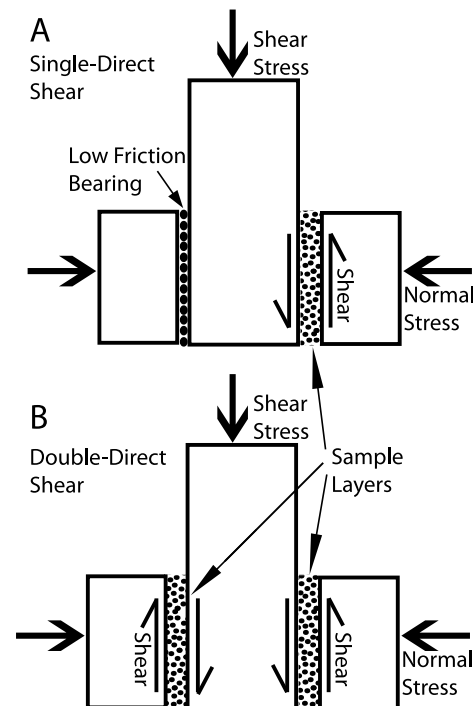


Figure 5. Experimental forcing block geometries for (a) single-direct shear (SDS) and (b) double-direct shear (DDS).

Table 3. Double-Direct Shear Experimental Parameters^a

Experiment	Normal Stress (MPa)	Shear Strain (γ)	Sliding Velocity ($\mu\text{m/s}$)	Saturated	Skewness	μ at Final Strain
p2143	0.7	0.67	10	No	0.15	0.584
p2132	0.7	16	10	No	0.63	0.641
p2130	0.71	6–7	10	Yes	0.91	0.492
p2127	0.7	unkn	10	No	0.53	0.604
p2141	0.7	7.65	30	No	0.50	0.615
p2300	0.75	2.57	100	No	0.32	0.588
p2142	0.71	8.58	100	No	0.46	0.586
p2302	0.75	0.58	300	No	0.28	0.599
p2301	0.76	2.23	300	No	0.39	0.568
p2303	0.74	2.6	1000	No	0.26	0.6
p2307	0.75	2.97	1000	No	0.46	0.619
p2156	0.98	0.65	10	No	0.32	0.55
p2146	0.97	10.39	10	Yes	0.95	0.587
p2149	1.02	17.52	10	No	0.80	0.562
p2128	0.92	7.77	10	No	Unkn	0.624
p2144	0.97	unkn	10	No	0.65	0.634
p2152	0.97	9.63	30	No	0.63	0.618
p2160	0.97	8.82	100	No	0.57	0.639
p2162	0.97	9.02	300	No	0.54	0.550
p2420	1.22	0.77	10	No	0.30	0.534
p2164	1.21	1.24	10	No	0.17	0.565
p2150	1.21	17	10	No	0.86	0.625
p2147	1.21	unkn	10	No	0.79	0.615
p2165	1.21	8.65	30	No	0.56	0.608
p2166	1.21	9.27	100	No	0.76	0.643
p2167	1.21	7.98	300	No	0.61	0.64
p2168	1.46	0.66	10	No	0.35	0.557
p2172	1.46	13.42	10	Yes	0.97	0.576
p2421	1.56	16.87	10	No	0.87	0.552
p2151	1.46	18.66	10	No	0.84	0.637
p2148	1.45	8.12	10	No	0.62	0.598
p2169	1.45	unkn	30	No	0.71	0.61
p2170	1.45	9.66	100	No	0.79	0.588
p2308	1.51	2.8	250	No	0.61	0.561
p2171	1.45	8.31	300	No	0.62	0.635
p2305	1.49	2.9	1000	No	0.63	0.599
p2306	1.49	3.63	1000	No	0.69	0.568
p2140	1.75	0.65	10	No	0.27	0.567
p2417	1.8	1.56	10	No	0.60	0.551
p2418	1.78	13.06	10	No	unkn	0.53
p2137	1.74	2.33	10	No	0.50	0.503
p2124	1.74	6.85	10	No	0.78	0.595
p2134	1.74	7.37	10	No	0.83	0.546
p2131	1.75	7.47	10	No	0.83	0.55
p2173	1.75	9.71	10	Yes	0.94	0.607
p2419	1.76	unkn	10	No	0.89	0.503
p2125	1.74	unkn	10	No	0.80	0.605
p2126	1.75	unkn	10	No	0.87	0.632
p2138	1.75	unkn	30	No	0.80	0.612
p2139	1.75	unkn	100	No	0.82	0.616
p2135	1.75	unkn	300	No	0.69	0.596

^aExperiments were conducted on parent material at constant sliding velocity (10 $\mu\text{m/s}$), normal stress (0.75–1.75 MPa), and moisture conditions (dry/saturated). We report the final shear strain, friction, and skewness for each experiment.

strength (Figure 8). Figure 8 compares the strength of the cataclastic shear bands to the strength of parent material for the duration of each SDS experiment ($\gamma = 0$ –20). The DDS experiments were designed to explore strain hardening of parent materials in greater detail.

3.2. Strain Hardening Behavior of Parent Material

[24] Parent material exhibits systematic strengthening and grain breakage as a function of shear strain under all conditions (Figures 9 and 10). The particle size of undeformed parent material is primarily 190–220 μm . Figure 9 shows decreased abundance of coarser grains (190–220 μm) and

increased abundance of finer grains (1–100 μm) as a function of shear strain. Figure 10 shows that parent material skewness and strength increase as a function of strain over a range of normal stresses (0.75–1.5 MPa). Strength increase and fine particle generation occur most readily early in experiments ($\gamma = 0$ –10) and become less pronounced as the experiments progress (Figure 10). In general, strengthening and fine particle generation are enhanced at higher normal stresses. Parent material strength and skewness (more fine particles) are positively related (Figure 10, insets).

[25] Fine particle generation is dramatically enhanced under saturated conditions. Figure 11 shows that saturated experiments have a pronounced abundance of fine grains

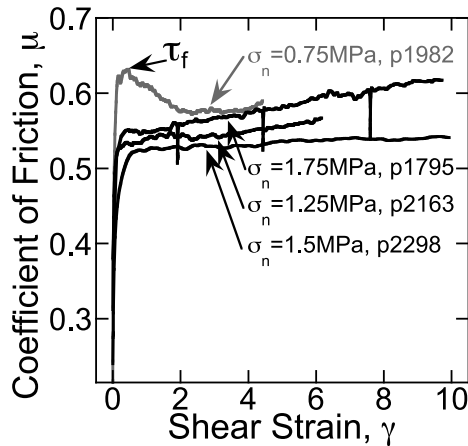


Figure 6. Coefficient of friction as a function of shear strain for representative experiments conducted on parent material (black lines) and cataclastic shear bands (gray line). For each experiment, we show normal stress (MPa) and experiment number (see Table 2 for other details). Maximum shear stress at the initiation of permanent shear deformation (τ_f) is shown for experiment p1982.

(1–100 μm) relative to dry experiments under otherwise identical experimental conditions. The PSDs from saturated experiments are similar to the cataclastic shear bands, both in terms of the 190–220 μm and 1–100 μm size fractions (Figure 11). Sheared parent material also appears similar to cataclastic deformation bands in thin section (Figure 12); the large grains tend to be subrounded, whereas the smaller grains tend to be angular. As well, sheared parent material and cataclastic shear bands have grain supported skeletons, where many grain contacts are surrounded by fine-grained matrix. The PSD in Figure 11 is representative of cataclastic shear bands and shows a distinct 0.3–0.4 μm size fraction. This size fraction is not observed in sheared parent material

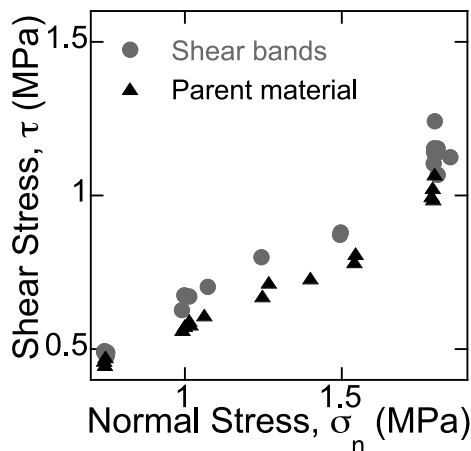


Figure 7. Coulomb-Mohr failure envelope showing τ_f as a function of normal stress for cataclastic shear bands ($\mu_i = 0.623$, $c_0 = 22$ kPa) and parent material ($\mu_i = 0.525$, $c_0 = 48$ kPa).

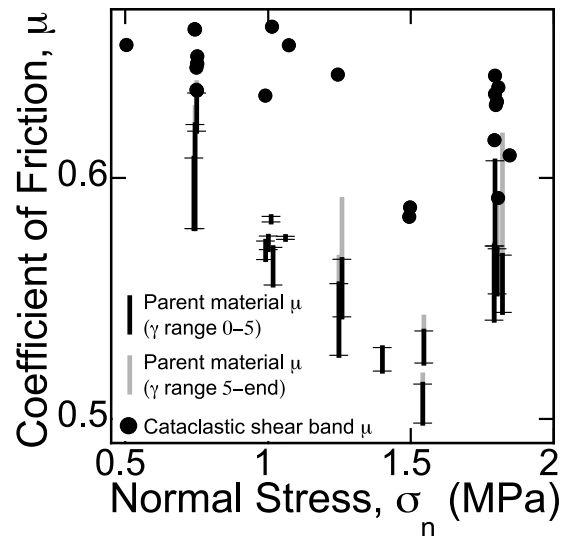


Figure 8. Friction during sliding for parent material and cataclastic shear bands. Values for parent material are shown for the initial portion of individual experiments (black bars) and for the remainder of the experiment (gray bars). Black dots show the maximum friction at the initiation of shear for cataclastic shear bands (τ_f divided by normal stress).

under any experimental conditions (Figure 11), which is a point we discuss below.

[26] Sliding velocity does not have a systematic effect on the behavior of parent material for our range of experimental conditions (Table 3). In particular, we analyzed the effect of velocity on τ_f and the rate of strain hardening, and did not find an effect. Inherent variation between samples, due to

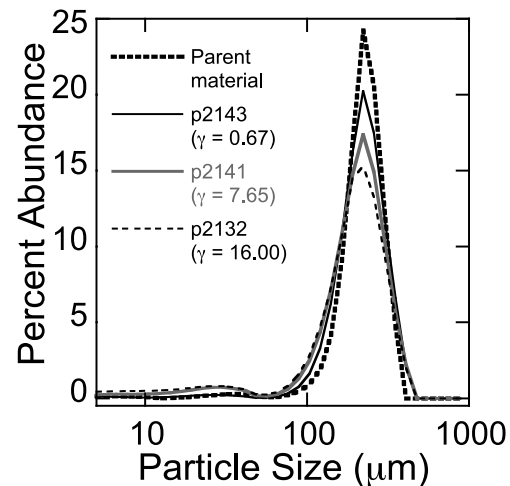


Figure 9. PSDs of parent material as a function of shear strain from dry experiments at $\sigma_n = 0.75$ MPa and shear velocity of 10 $\mu\text{m/s}$; 220 μm represents the most abundant size. Note that the peak abundance decreases systematically as a function of shear strain. This decrease abates with increasing shear strain.

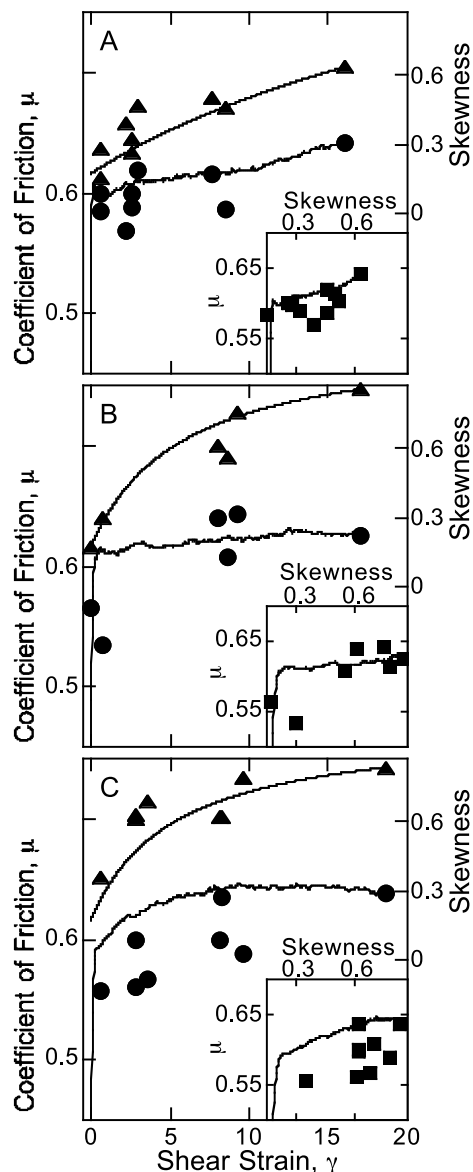


Figure 10. [Main plots] Friction (circles) and skewness (triangles) as a function of shear strain at normal stresses of (a) 0.75, (b) 1.25, and (c) 1.5 MPa. Skewness and friction values are reported from the end of individual experiments ($\gamma = 0$ –20). Details of skewness and friction as a function of γ are shown at each normal stress. [Insets] Friction as a function of skewness at the end of each experiment (squares). Details of friction as a function of skewness are shown at each normal stress.

material heterogeneity or experiment procedures, may have a greater effect on parent material behavior than slip velocity.

4. Discussion

[27] Our results show that cataclastic shear bands are stronger than parent material. This strength difference is particularly evident at the onset of permanent shear defor-

mation (Figures 6 and 7). These data imply that, once cataclastic shear bands form, they will not reactivate to accommodate additional strain. Instead, additional strain will be accommodated within nearby parent material. An intuitive result of this behavior is networks of closely spaced cataclastic deformation bands, as has been posited by previous researchers for sandstones [Aydin, 1978; Schulz and Balasko, 2003]. Our results demonstrate that this explanation also applies to unlithified sand.

4.1. The Role of Grain Breakage

[28] Grain breakage of parent material occurs over our full range of experimental conditions as indicated by the decreased abundance of coarser grains (190–220 μm) and increased abundance of finer grains (1–100 μm) with strain. Grain breakage is observable during parent material experiments in the form of short-term chaotic frictional behavior (Figure 6). Similar data have been described previously [Fedá, 2002; Lobo-Guerrero and Vallejo, 2005; Guo and Morgan, 2006]. Fedá [2002] describes these as garland like friction curves, which are attributed to grain breakage or cyclic softening associated with force chain failure and reorganization of a new load bearing skeleton.

[29] Progressive grain breakage results in strain hardening of parent material as indicated by the positive correlation of skewness (more fine particles) and strength (Figure 10). Grain breakage results in strain hardening in three possible ways: (1) It generates finer grains (Figures 9 and 11; Table 3), which are expected to be stronger than larger grains, according to Petch's law [Petch, 1953]. (2) Finer grains fill in pore space, effectively increasing the grain coordination number and widening the PSD, each of which cause strengthening [Sammis et al., 1987]. (3) Grain breakage generates angular grains, which have been found to increase the frictional strength of granular materials [Lambe and

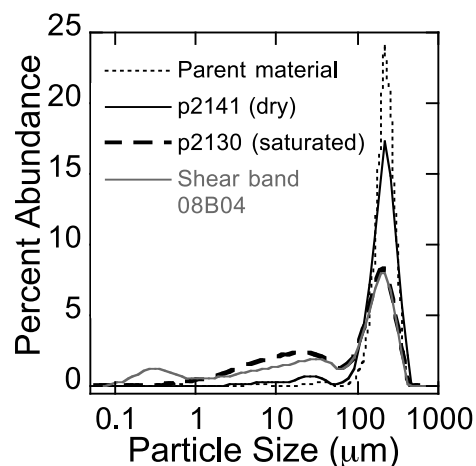


Figure 11. Particle size distributions of parent material, a cataclastic shear band (08B04; $\gamma = 5$), and parent material from saturated (p2130; $\gamma = 6$ –7) and dry (p2141; $\gamma = 7.65$) experiments conducted at 0.75 MPa normal stress. The PSD from the saturated experiment shows fewer coarser grains and an increased abundance of finer grains (1–100 μm) relative to the dry sample (p2141). The PSDs for the saturated experiment and cataclastic shear band are similar.

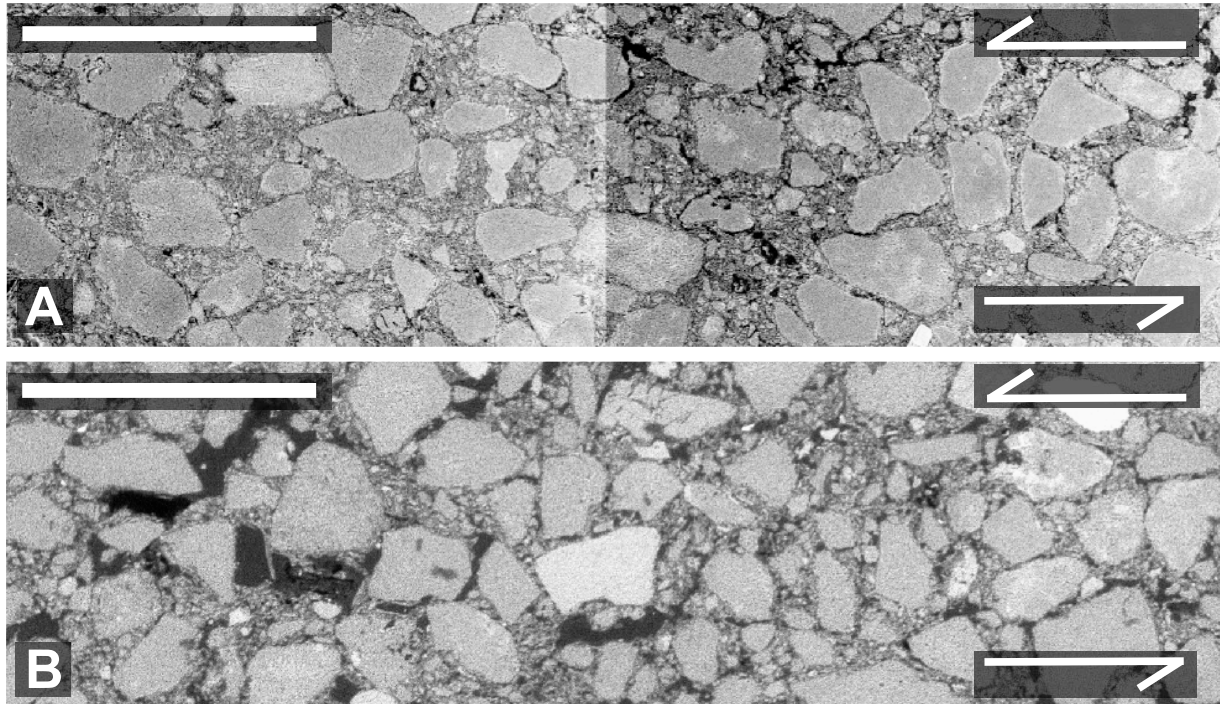


Figure 12. Oriented SEM images of (a) a cataclastic shear band (08C05; $\gamma = 6$) and (b) parent material from a saturated parent material experiment (p2130; $\gamma = 6-7$; $\sigma_n = 0.75$ MPa). Arrows denote sense of shear. Note similarities in grain size and morphology (see also Figure 11). Scale bars, 500 μm .

Whitman, 1969; Mair *et al.*, 2002; Anthony and Marone, 2005]. In our experiments, angular grains are generated by fracture of the subrounded parent grains (Figure 12).

[30] Grain breakage readily occurs early in experiments and becomes less prominent with strain. This is indicated by the large initial ($\gamma = 0-5$) increase in skewness followed by much less change at higher strains (Figure 10). Deformation via grain breakage decreases in favor of frictional grain boundary sliding, following the least energy intensive deformation mechanism. Grain breakage makes frictional sliding less energy intensive, because dilation of finer grains, if shear is localized, requires a smaller increase in layer thickness. In contrast, further grain breakage becomes more energy intensive, because finer grains are generally stronger, and the grain coordination number is increased. In effect, the fine grains generated by grain breakage promote dilation and frictional grain boundary sliding instead of continued grain breakage.

4.2. Cataclastic Shear Band Formation

[31] Parent material begins to develop a number of deformation-band-like characteristics during our experiments. In particular, parent material approaches cataclastic deformation band strength, especially at high shear strains ($\gamma = 20$; Figure 8). The particle size distribution of sheared parent material becomes similar to that of cataclastic deformation bands (Figure 11). In addition, sheared parent material becomes visually similar to the bands, including many large grains surrounded by pore space that is filled in by matrix (Figure 12). In particular, both sheared parent

material and cataclastic shear bands have grain supported skeletons, where many grain contacts are surrounded by fine-grained matrix.

[32] Under dry experimental conditions, the frictional strength of parent material approaches, but does not reach, the strength of cataclastic shear bands (Figure 8). The same is true for the particle size distribution of parent material and the cataclastic shear bands (Figure 11). The differences

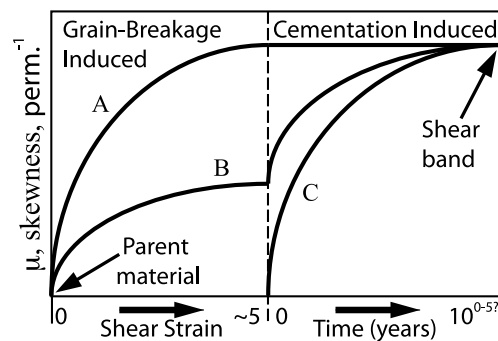


Figure 13. Possible evolution paths (μ , skewness and permeability) of cataclastic shear bands developing from parent material. Model A is a case where band characteristics develop due to grain breakage. Model C is a case where band characteristics develop due to cementation. Model B, our preferred model, is a case where cataclastic shear band characteristics develop initially by grain breakage, and are later modified by cementation.

in strength and PSD are likely due to differences in laboratory versus natural sliding conditions (e.g., diagenesis, cementation, or sliding velocity). One could argue that shear strain is a factor; however, our laboratory experiments reached shear strains of up to 20, which is similar to the field estimates for the natural bands. Normal stress is another potential variable; however, our experiments were conducted at normal stresses near the upper end of the likely range of in situ normal stress (1.8 MPa), and thus this does not appear to be a likely explanation.

[33] Under saturated experimental conditions, parent material develops a PSD remarkably similar to cataclastic shear bands (Figure 11). This similarity is highlighted by a decrease in the 190–220 μm and increase in the 1–100 μm size fraction relative to dry experiments under otherwise identical experimental conditions. These PSD differences arise from an increased propensity for granular fracture under saturated conditions, which is consistent with the effect of hydrolytic weakening on fracture [e.g., *Miura and Yamanouchi*, 1975].

[34] Cataclastic shear bands have a greater proportion of fine particles, in the range 0.3–0.5 μm , than virgin or sheared parent material (Figure 11). These particles represent a fraction below the 1 μm mechanical grinding limit suggested by *Sammis and Ben-Zion* [2008]. Diagenesis and/or clay accumulation by filtration of groundwater could account for fine particles and would indicate that cataclastic shear bands evolve through time. Subcritical crack growth and fragmentation, aided by hydrolytic weakening, could also account for particles finer than 1 μm and might occur shortly after band formation. Another possible explanation for particles finer than 1 μm is coseismic, shock loading; however, we do not have additional supporting evidence for this.

4.3. The Role of Diagenesis

[35] We posit that cementation accounts for the differences in strength and PSD between the cataclastic shear bands and experimentally sheared parent material. Our data show that the bands have higher initial frictional strength than parent material (Figure 6). Cataclastic shear bands also exhibit postpeak weakening, in contrast to the strain hardening observed in parent material. Cementation may arise in nature from iron oxide and clay accumulation [*Cresswell and Barton*, 2002], which may be enhanced in the bands due to their decreased porosity and permeability relative to parent material. *Du Bernard et al.* [2002] have argued that clay accumulation plays a role in dilation bands, and thus, it may be a factor in our shear bands. Similarly, iron oxide precipitation is pervasive at our study site (Figure 2) and may be enhanced in cataclastic deformation bands via preferred water retention, which may increase the kinetics of chemical weathering and enhance cementation.

4.4. Strain Hardening and Localization Within Cataclastic Shear Bands

[36] A fundamental question about the mechanics of cataclastic shear bands involves how localization can be sustained in a strain-hardened zone that is adjacent to weaker material. For cataclastic shear band formation in sandstones, previous workers have noted the importance of an initial strain weakening mechanism such as cohesive breakdown [*Mair et al.*, 2000; *Lothe et al.*, 2002]. However, the

application of cohesive breakdown to unlithified sand is unclear. In particular, our experiments do not show consistent strain weakening behavior of parent material. In their present state, our deformation bands are stronger and have enhanced cohesive strength compared to the surrounding parent material. However, they presumably formed from parent material, prior to acquiring increased cohesion. Our experiments suggest that cataclastic shear band formation is associated with either grain fracture, causing local weakening, or a mechanism associated with the propagation of a coseismic shear rupture from a nearby lithified unit [e.g., *Cashman and Cashman*, 2000; *Wen and Aydin*, 2004; *Cashman et al.*, 2007].

5. Conclusions

[37] Our results are consistent with the hypothesis that cataclastic deformation bands are stronger than their parent material. We find that the relative strength of cataclastic shear bands is largely a result of strain hardening via shear driven grain breakage. Pervasive grain breakage results in strengthening via increased grain angularity and fine particle abundance. As shear progresses, grain breakage (and strength increase) abates in favor of steady state grain boundary sliding. Although grain breakage results in increased material strength, it cannot account for the full strength difference between cataclastic shear bands and their parent material. Given this strength discrepancy and the presence of clay sized particles (<1 μm), we posit that cementation acts to further increase the strength of cataclastic deformation bands (Figure 13). Preferential cementation of cataclastic deformation bands, relative to the surrounding parent material, has important implications for flow paths, permeability, and strength in poorly lithified sands.

[38] **Acknowledgments.** We thank Andy Rathbun and Enrique Perez for assistance in the field and Samuel Haines for assistance with SEM analysis. We gratefully acknowledge support from NSF grants REU EAR 0545702, EAR 0746192, and OCE 0648331.

References

- Anthony, J. L., and C. Marone (2005), Influence of particle characteristics on granular friction, *J. Geophys. Res.*, *110*, B08409, doi:10.1029/2004JB003399.
- Antonellini, M. A., A. Aydin, and D. D. Pollard (1994), Microstructure of deformation bands in porous sandstones at Arches National Park, Utah, *J. Struct. Geol.*, *16*(7), 941–959.
- Aydin, A. (1978), Small faults formed as deformation bands, *Pure Appl. Geophys.*, *116*, 913–930.
- Aydin, A. (2000), Fractures, faults, and hydrocarbon entrapment, migration and flow, *Mar. Pet. Geol.*, *17*, 797–814.
- Aydin, A., R. I. Borja, and P. Eichhubl (2006), Geological and mathematical framework for failure modes in granular rock, *J. Struct. Geol.*, *28*, 83–98.
- Berger, G. W. (1992), Thermoluminescence dating of coastal sediments near Eureka, in *Friends of the Pleistocene Field Trip Guidebook*, Pac. Cell.
- Bonn, D., and M. M. Denn (2009), Yield stress fluids slowly yield to analysis, *Science*, *324*, 1401–1402, doi:10.1126/science.1174217.
- Borja, R. I. (2004), Computational modeling of deformation bands in granular media: II. Numerical simulations, *Comp. Meth. Appl. Mech. Eng.*, *193*, 2699–2718.
- Borja, R. I., and A. Aydin (2004), Computational modeling of deformation bands in granular media. I. Geological and mathematical framework, *Comp. Meth. Appl. Mech. Eng.*, *193*, 2667–2698.

- Carver, G. A., and R. M. Burke (1992), Late Cenozoic deformation on the Cascadia subduction zone in the region of the Mendocino Triple Junction, *Friends of the Pleistocene Field Trip Guidebook*, Pac. Cell.
- Cashman, S. M., and K. V. Cashman (2000), Cataclasis and deformation-band formation in unconsolidated marine terrace sand, Humboldt County, California, *Geology*, 28(2), 111–114.
- Cashman, S. M., J. M. Baldwin, K. V. Cashman, K. Swanson, and R. Crawford (2007), Microstructures developed by coseismic and aseismic faulting in near-surface sediments, San Andreas fault, California, *Geology*, 35(7), 611–614.
- Clarke, S. H., and G. A. Carver (1992), Late Holocene tectonics and paleoseismicity, southern Cascadia subduction zone, *Science*, 255, 188–192.
- Cresswell, A. W., and M. E. Barton (2002), Direct shear tests of an uncemented, and a very slightly cemented, locked sand, *Q. J. Eng. Geol.*, 36, 119–132.
- Du Bernard, X., P. Eichhubl, and A. Aydin (2002), Dilation bands: A new form of localized failure in granular media, *Geophys. Res. Lett.*, 29(24), 2176, doi:10.1029/2002GL015966.
- Feda, J. (1982), *Mechanics of Particulate Materials*, Dev. Geotech. Eng., vol. 30, Elsevier, New York.
- Feda, J. (2002), Notes on the effect of grain crushing on the granular soil behaviour, *Eng. Geol.*, 63, 93–98.
- Folk, R. L., and W. C. Ward (1957), Brazos river bar: A study in the significance of grain size parameters, *J. Sediment. Res.*, 27, 3–26.
- Fossen, H., R. A. Schultz, Z. K. Shipton, and K. Mair (2007), Deformation bands in sandstone: A review, *J. Geol. Soc.*, 164, 755–769.
- Guo, Y., and J. K. Morgan (2006), The frictional and micromechanical effects of grain comminution in fault gouge from distinct element simulations, *J. Geophys. Res.*, 111, B12406, doi:10.1029/2005JB004049.
- Harvey, E. (1994), Late Pleistocene sediments and fossils near the mouth of Mad River, Humboldt County, California: Facies analysis, sequence development, and possible age correlation, unpublished, M.S. thesis, 66 pp., Hum. St. Univ., Arcata, Calif.
- Knudsen, F. P. (1959), Dependence of mechanical strength of brittle polycrystalline specimens on porosity and grain size, *J. Am. Ceram. Soc.*, 42(8), 376–387.
- Lambe, T. W., and R. V. Whitman (1969), *Soil Mechanics*, pp. 33–39, John Wiley, New York.
- Lobo-Guerrero, S., and L. E. Vallejo (2005), Analysis of crushing of granular material under isotropic and biaxial stress conditions, *Soils Found.*, 45(4), 79–87.
- Lothe, A. E., R. H. Gabrielsen, N. Bjørnevoll Hagen, and B. T. Larsen (2002), An experimental study of the texture of deformation bands: Effects on the porosity and permeability of sandstones, *Petrol. Geosci.*, 8, 195–207.
- Mair, K., I. Main, and S. Elphick (2000), Sequential growth of deformation bands in the laboratory, *J. Struct. Geol.*, 22, 25–42.
- Mair, K., K. Frye, and C. Marone (2002), Influence of grain characteristics on the friction of granular shear zones, *J. Geophys. Res.*, 107(B10), 2219, doi:10.1029/2001JB000516.
- Marone, C. (1995), Fault zone strength and failure criteria, *Geophys. Res. Lett.*, 22(6), 723–726, doi:10.1029/95GL00268.
- Marone, C. (1998), Laboratory-derived friction laws and their application to seismic faulting, *Annu. Rev. Earth Planet. Sci.*, 26, 643–696.
- Marone, C., B. M. Carpenter, and P. Schiffer (2008), Transition from rolling to jamming in thin granular layers, *Phys. Rev. Lett.*, 101(24), 8001, doi:10.1103/PhysRevLett.101.248001.
- Miura, N., and T. Yamanouchi (1975), Effect of water on the behavior of a quartz-rich sand under high stress, *Soils Found.*, 15(4), 23–34.
- Parnell, J., G. R. Watt, D. Middleton, J. Kelly, and M. Baron (2004), Deformation band control on hydrocarbon migration, *J. Sediment. Res.*, 74(4), 552–560.
- Perez, E., B. M. Kaproth, S. H. Haines, and D. Saffer (2010), laboratory measurements of permeability reduction in naturally occurring shear bands formed in unlithified sands, *Geol. Soc. Am. Abstr. Programs*, 42(4), Abstract 172868.
- Petch, N. J. (1953), The cleavage strength of polycrystals, *J. Iron Steel Inst.*, 174, 25–28.
- Rathbun, A. R., C. Marone, R. B. Alley, and S. Anandakrishnan (2008), Laboratory study of the frictional rheology of sheared till, *J. Geophys. Res.*, 113, F02020, doi:10.1029/2007JF000815.
- Rawling, G. C., and L. B. Goodwin (2003), Cataclasis and particulate flow in faulted, poorly lithified sediments, *J. Struct. Geol.*, 25, 317–331.
- Sammis, C. G., and Y. Ben-Zion (2008), Mechanics of grain-size reduction in faults, *J. Geophys. Res.*, 113, B02306, doi:10.1029/2006JB004892.
- Sammis, C. G., G. King, and R. Biegel (1987), The kinematics of gouge deformation, *Pure Appl. Geophys.*, 125(5), 777–812.
- Savage, H. M., and C. Marone (2007), Effects of shear velocity oscillations on stick-slip behavior in laboratory experiments, *J. Geophys. Res.*, 112, B02301, doi:10.1029/2005JB004238.
- Schultz, R. A., and C. M. Balasko (2003), Growth of deformation bands into echelon and ladder geometries, *Geophys. Res. Lett.*, 30(20), 2033, doi:10.1029/2003GL018449.
- Scott, D. R., C. Marone, and C. G. Sammis (1994), The apparent friction of granular fault gouge in sheared layers, *J. Geophys. Res.*, 99(B4), 7231–7246, doi:10.1029/93JB03361.
- Wen, B. P., and A. Aydin (2004), Deformation history of a landslide slip zone in light of soil microstructure, *Environ. Eng. Geosci.*, 10(2), 123–149.
- Wong, T.-F., H. Szeto, and J. Zhang (1992), Effect of loading path and porosity on the failure mode of porous rocks, *Appl. Mech. Rev.*, 45, 281–293, doi:10.1115/1.3119759.
- Wong, T.-F., C. David, and B. Menéndez (2004), Mechanical compaction, in *Mechanics of Fluid Saturated Rocks*, edited by Y. Guéguen, and M. Boutéca, pp. 55–114, Elsevier, Amsterdam.
- Zhu, W., and T.-F. Wong (1997), The transition from brittle faulting to cataclastic flow: Permeability evolution, *J. Geophys. Res.*, 102(B2), 3027–3041, doi:10.1029/96JB03282.
- Zhu, W. L., L. G. J. Montesti, and T. F. Wong (1997), Shear-enhanced compaction and permeability reduction: Triaxial extension tests on porous sandstone, *Mech. Mater.*, 25(3), 199–214.

S. M. Cashman, Department of Geology, Humboldt State University, Arcata, CA 95521, USA.

B. M. Kaproth and C. Marone, Department of Geosciences, Pennsylvania State University, 522 Deike Bldg., University Park, PA 16802, USA. (bkaproth@psu.edu)